Processing and Application of Ceramics 14 [2] (2020) 119–127
https://doi.org/10.2298/PAC2002119Q



# Structural and optical properties of Al-doped ZnO thin films produced by magnetron sputtering

José César Augusto de Queiroz[1,*], João Batista de Azevedo Filho[2], José Quinzinho de Medeiros Neto[1], Igor Oliveira Nascimento[1], Ivan Alves de Souza[1], Maria Gerlania de Oliveira Queiroz[3], Emanuel Benedito de Melo[4], José Daniel Diniz Melo[1], Thercio Henrique de Carvalho Costa[1]

[1]*Mechanical Engineering Department, Federal University of Rio Grande do Norte, University Campus, Natal, RN, Brazil*
[2]*Institute of Chemistry, Federal University of Rio Grande do Norte, University Campus, Natal, RN, Brazil*
[3]*Federal Rural University of the Semi-Arid, Pau dos Ferros, RN, Brazil*
[4]*Federal Institute of Education Science and Technology of São Paulo, São Paulo, SP, Brazil*

Received 17 November 2019; Received in revised form 6 February 2020; Accepted 27 March 2020

## Abstract

*Experimental and theoretical investigations of the structure and optical properties of Al-doped ZnO (AZO) thin films produced by magnetron sputtering under different values of electric current were conducted. The XRD results confirm the formation of the AZO thin films with hexagonal wurtzite structure, with preferential orientation along the crystallographic plane (002), direction c. The increment of electric current allowed an increase in average crystallite size. The FE-SEM and AFM images analyses of the AZO films revealed the occurrence of nucleation on the substrate surface that formed films with granular and rough structure. The higher substrate temperature caused by the higher value of electric current had influence on the grain size and thickness (ranging from 974 to 1500 nm) of the formed thin films. Due to the high absorption of free carriers, the optical transmittance of the AZO films was acceptable for the visible spectrum and limited to the near infrared region. The energy band gap values for both AZO films, measured from the optical transmission spectra, were ideal for semiconductor applications. The ab initio calculations using DFT and the method LSDA + U along with the correction of Hubbard were successfully applied to investigate the structural and optical effects. The band structures of the pure ZnO and ZnO:Al, calculated in this work, presented $E_g$ values close to the experimental results. Therefore, these results imply that our methods are reliable and that the calculations are in accordance with the experimental results.*

***Keywords:*** *AZO thin films, magnetron sputtering, energy band diagram, ab initio calculation*

## I. Introduction

Recently, new materials for semiconductor applications have been widely researched. These materials are promising for the production of piezoelectric and optical devices, both triggered by electrical and magnetic fields [1]. These materials have a multifunctional character with optical transparency and good electrical conductivity, so they can be used in conductive electrodes and solar cell surfaces, among others [2,3]. In this context, transparent conductive oxides (TCO) thin films are alternatives that can satisfy certain demands according to their electrical nature (presenting conductivity of p- or n-type, depending on the doping chosen to be incorporated in the TCO lattice) [4], as well as its high optical transparency, in relation to the range of the visible spectrum [2–5].

The transparent oxides that have been receiving great attention are ZnO:Al (AZO) and $SnO_2$:F (FTO), due to their electrical and optical properties [6,7]. AZO is constituted by elements of group II–VI from the periodic table, with wide energy band gap value (3.34 eV) of di-

*Corresponding author: tel: +55 84 99167 6596,
e-mail: *jose.cesar@ufrn.edu.br*

rect nature, wurtzite structure and it has been successfully applied due to its photocatalytic properties [8,9]. In addition, high electrical conductivity and low toxicity of ZnO attract researchers' attention since it is a transparent conductive oxide [6,8–10].

AZO has been intensively studied in the form of thin films, since it has a low electrical resistivity associated with a high optical transmittance [11,12]. AZO thin films are usually synthesized by spraying reactions and the synthesis conditions have been reported as the most important factor for the formation of the crystalline structure, going from Wurtzite ($P6_3mc$) to Rock salt ($Fm3m$) at high pressures and from Rock salt to Zincblende ($F43m$) through epitaxial growth synthesis on a substrate with cubic crystalline structure [13]. Current studies on AZO thin films have concentrated on the verification of rules that can govern the doping and synthesis processes, aiming to obtain a semiconductor material [14]. The synthesis conditions determine the atomic order of the sub-lattice and as a result, they also affect the electrical and optical properties of AZO thin films [15]. When $Al^{3+}$ ions replace the $Zn^{2+}$ ions, the sites belonging to the wurtzite structure are contracted since the Al–O bond is stronger than the Zn–O bond. In addition, $Al^{3+}$ with a smaller ionic radius, strongly connected to the network, forces the contraction of the site and promotes the decrease of the lattice parameters $a$ and $c$ [16]. The Density Functional Theory (DFT) calculations propose that AZO is an n-type semiconductor [17], generated by the ion-substitution in the crystal structure, which causes possible distortions and defects in crystalline lattice [16–18].

In the present study, the structure and optical properties of AZO thin films were investigated in an experimental and theoretical way, aiming to better understand the structural and optical ordering of this material.

## II. Experimental procedure

### 2.1. Deposition of thin films

The ZnO:Al thin films were prepared by physical vapour deposition (DC magnetron sputtering) [19] on a glass substrate. The design of the deposition system was based on the theory and configurations presented in the literature [20]. The substrates were immersed in acetone, distilled water and isopropyl alcohol using an ultrasonic bat and dried with an air jet. The base pressure in the deposition chamber was maintained at $\sim 1 \times 10^{-4}$ mbar with a diffusion pump and the gas used in the process was argon (purity of 99.999%) at a flow rate of 10 $cm^3$/min. The gas flow was manipulated through a mass flow controller (MKS Instruments model). The target-substrate distance was constant and equal to 4 cm. The ceramic target (99.99% purity, $ZnO:Al_2O_3$ = 98:2 wt.%) with diameter of 50.8 mm and thickness of 6.35 mm, purchased from ACI ALLOYS, was used. Two Al-doped zinc oxide thin films were produced, AZO-1 and AZO-2, using working current of 0.3 and 0.4 A, respectively. The deposition time of 0.5 h and temperature of 90 °C were used in both cases. To apply the potential difference and maintain the active plasma, a square wave pulsed current source was employed. In order to remove the oxide layer and possible impurities present on the surface of the AZO target, it was subjected to a pre-sputtering process, for 30 min, at a pressure of $4 \times 10^{-3}$ mbar and air gas flow rate of 20 $cm^3$/min.

### 2.2. Characterization

The microstructure and crystallographic phases, present in the AZO films, were analysed by X-ray diffraction equipment (BRUKER, D2 PHASER), using CuK$\alpha$ radiation ($\lambda$ = 0.15406 nm). The crystallite sizes ($D$) were calculated using the Debye-Sherrer equation [21]:

$$D = \frac{k \cdot \lambda}{\beta \cdot \cos\theta} \quad (1)$$

where $k$ is the Scherrer constant (0.90), $\lambda$ represents the wavelength of X-rays (0.15406 nm), $\beta$ is the full-width at half-height of the X-ray diffraction peak (FWHM) and $\theta$ is the Bragg diffraction angle.

The surface morphology and the topographic profile of the samples were measured by scanning electron microscope with field emission gun (EGF-Inspect F50) and an atomic force microscope (SHIMADZU) using the intermittent contact mode.

The optical characterization of the deposited films was performed in the range from 300 to 1100 nm using a spectrophotometer (Genesys). Optical transmittance measurements were used to estimate the band gap energy of the AZO thin films.

### 2.3. Procedure for the first principle calculations

The calculations of the electronic structure of the AZO thin films, under ambient conditions of temperature and pressure, were made using a 2 × 2 × 2 super cell, generated from the experimental unit cell of ZnO (wurtzite). The software Quantum Espresso 6.2 was used for the calculation [22,23] based on the Density Functional Theory (DFT) [24], using the generalized gradient approximation (GGA) with the Perdewe-Burke-Ernzerhof (PBE) [25] functional being considered for the Exchange-correlation effects. The electron-ion interactions were described by Projector Augmented Wave (PAW). The cut for the kinetic energy was 50 Ry and for the charge density it was 500 Ry. The set of points on the irreducible Brillouin zone (BZ) was 328 $k$-points distributed on dimension grade FFT (60, 60, 81) using the Monkhorst-Pack scheme [26]. The pseudopotentials used to describe the interaction between nucleus and valence electrons were from the norm-conserving (NCPP) Troullier-Martins method [27]. For the Zn, Al and O elements, the pseudopotentials Zn.pbe-mt_fhi.UPF, Al.pbe-mt_fhi.UPF and O.pbe-mt_fhi.UPF were used, respectively. The BFGS algorithm was applied to relax the whole crystal in order to reach the

ground state configuration. For the convergence tolerance of the calculation, the authors used: energy of $5.0 \times 10^{-6}$ eV/atom, maximum force on each atom of 0.01 eV/Å, applied pressure of 0.05 GPa and maximum atomic displacement of $5.0 \times 10^{-4}$ Å. To generate the unit cell and the electronic density images, the group used the software package Burai 1.3 from Satomichi Nishihara and VESTA 3 [28].

## III. Results and discussion

### 3.1. Structure of AZO films

Figure 1 shows XRD patterns of the AZO thin films. The diffractograms confirm the formation of Al-doped ZnO (Al:ZnO) by the presence of the peak at $2\theta = 34.0°$ for the AZO-1 film and $2\theta = 33.6°$ for the AZO-2 film that are indexed to the hexagonal wurtzite structure according to the crystallographic chart 1537875 of the Crystallography Open Database (COD). The absence of diffraction peaks related to Al and $Al_2O_3$ phases suggests a deposition process with a high AZO degree of purity, for current and voltage variations. Thus, the ions of $Al^{3+}$ replace the $Zn^{2+}$ ions in the structure of the hexagonal wurtzite and they can also occupy the interstices or segregate in the grain boundary region [29]. The X-ray diffraction patterns are dominated by intense peaks related to the crystallographic plane (002) indicating the formation of the doped ZnO with high texture along the direction [001] [30].

Table 1 reports the values of the deposition rate, FWHM and crystallite size for the AZO thin films. The increase in the value of the deposition current results in the increase of the crystallite size, which promotes the decrease in the number of grains and, consequently, an increase in the grains oriented along the direction [001]. This elevates the degree of crystallinity for the AZO films [31]. The reduction of the FWHM value (from 0.315° to 0.241°) indicates an improvement in the crystallinity and increase in crystallite sizes (from 20.55 to 40.32 nm).

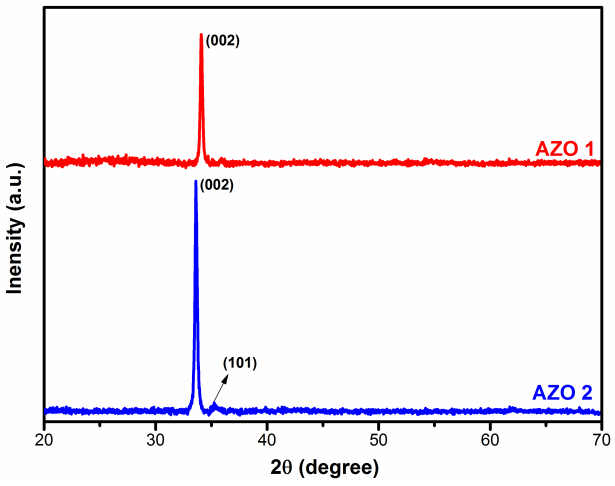


**Figure 1. XRD spectra of ZnO:Al thin films grown under different sputtering electric currents**

**Table 1. Result of deposition rate, FWHM and crystallite size (*D*) of AZO films deposited using: a) 0.3 A and 10 cm³/min and b) 0.4 A and 10 cm³/min**

| Film | Deposition rate [nm/min] | FWHM [°] | *D* [nm] |
|---|---|---|---|
| AZO-1 | 18.2 | 0.315 | 20.6 |
| AZO-2 | 22.5 | 0.240 | 40.3 |

FE-SEM images of the AZO thin films, deposited with current values of 0.3 A (AZO-1) and 0.4 A (AZO-2), are shown in Fig. 2. During the deposition process, nucleation occurs on the surface of the substrate, resulting in the formation of small crystals. The set of crystals forms a granular and rough structure and the presence of ZnO nanoparticles with irregular topographic profile for both deposition conditions characterize the AZO films, which is in accordance with literature data [32–34].

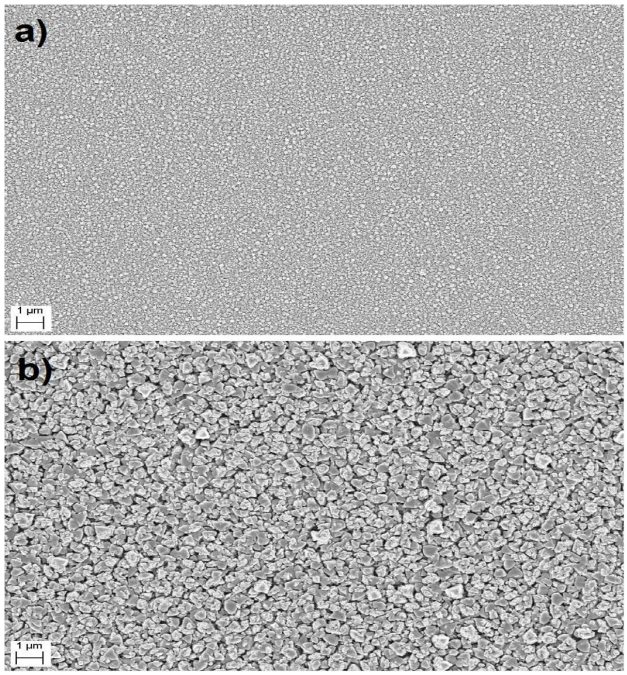


**Figure 2. FE-SEM micrographs of: a) AZO-1 and b) AZO-2 thin films**

From Fig. 2, it can be observed that the increase in the electric current caused an increase in the substrate temperature which, in turn, allowed the formation of the films with larger grain sizes due to the high diffusion energy [35]. Thin films with larger grain size decrease the influence of grain boundaries on the scattering of radiation and still contribute to the significant improvements in electrical properties [36].

Figure 3 presents FE-SEM images of the cross-sectional structure of the AZO thin films. It is possible to notice a columnar growth perpendicular to the glass substrate, characteristic of the polycrystalline AZO structure. The AZO-2 film has the thickness values of approximately 1500 nm while the AZO-1 film has lower thickness values. The electric current used to produce the AZO thin films promoted a high degree of thermal energy to the substrate, responsible for the coalescence

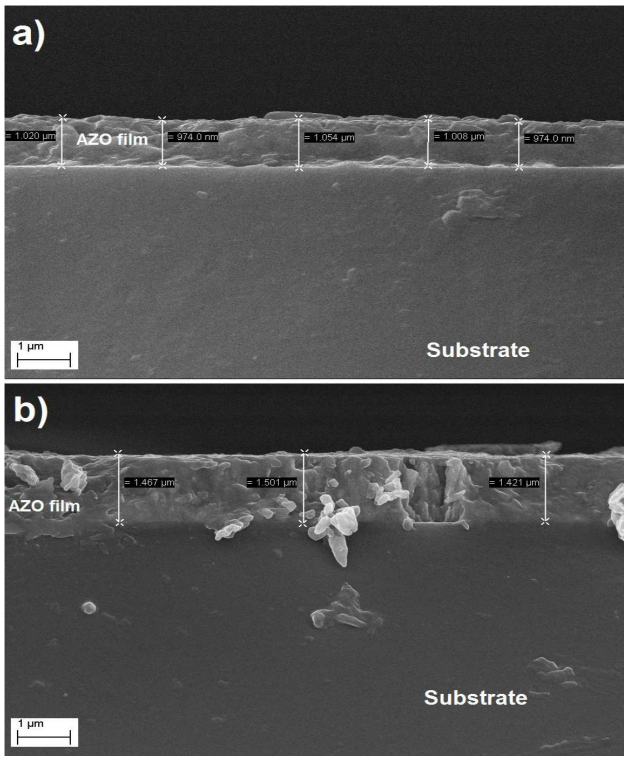


**Figure 3. Transverse FE-SEM images of: a) AZO-1 and b) AZO-2 thin films with thickness measurements along the structure of the films**

of the grains and crystallinity of the films. The AZO-2 film, deposited with the current of 0.4 A, has higher average thickness, due to the high deposition rate, high degree of crystallinity, as confirmed by X-ray diffraction, and better optical transmittance.

The three-dimensional AFM images with height profile are shown in Fig. 4, which compares the surface morphology of AZO thin films. The variation of the film roughness was attributed to the different deposition current. The surface of the AZO-2 film has higher roughness due to the formation of columnar structures, originated from the growth of the grains oriented along the direction [001]. One can observe a variation in the roughness of the AZO-1 film with formation of peaks, but in smaller quantity. The roughness variation of the AZO-1 and AZO-2 films can be associated with the different values of electric current used in the deposition process.

### *3.2. Optical properties*

Optical transmittance spectra of the films as well as the values of the absorption coefficient as a function of photons energy are shown in Fig. 5. The films exhibit high average transmittance (~75%) in the visible region. The AZO-2 film has higher optical transmittance (>80%) in the visible range as well as a low optical absorption coefficient in relation to the sample AZO-1. This optical behaviour suggests that the AZO thin films present relevant optical quality due to the low loss of radiation by dispersion or absorption [37]. The high values of optical transmittance are consistent with the results of the grain size, presented in Table 1. The crystalline structure of the film has direct influence on the interaction between the radiation and matter, since the grain boundary absorbs incident visible light, decreasing the percentage of the light that is transmitted through the structure of the film [38,39].

Thus, in order to calculate the band gap energy ($E_g$) of the AZO thin films, the values of optical absorption coefficient, presented in Fig. 5, were used, since it can be calculated by the following equation:

$$\alpha = \frac{1}{d} \cdot \ln \frac{1}{T} \tag{2}$$

where $T$ is the transmittance and $d$ is the thickness of the thin film layer. The relationship between the optical absorption coefficient and the energy of the photon for

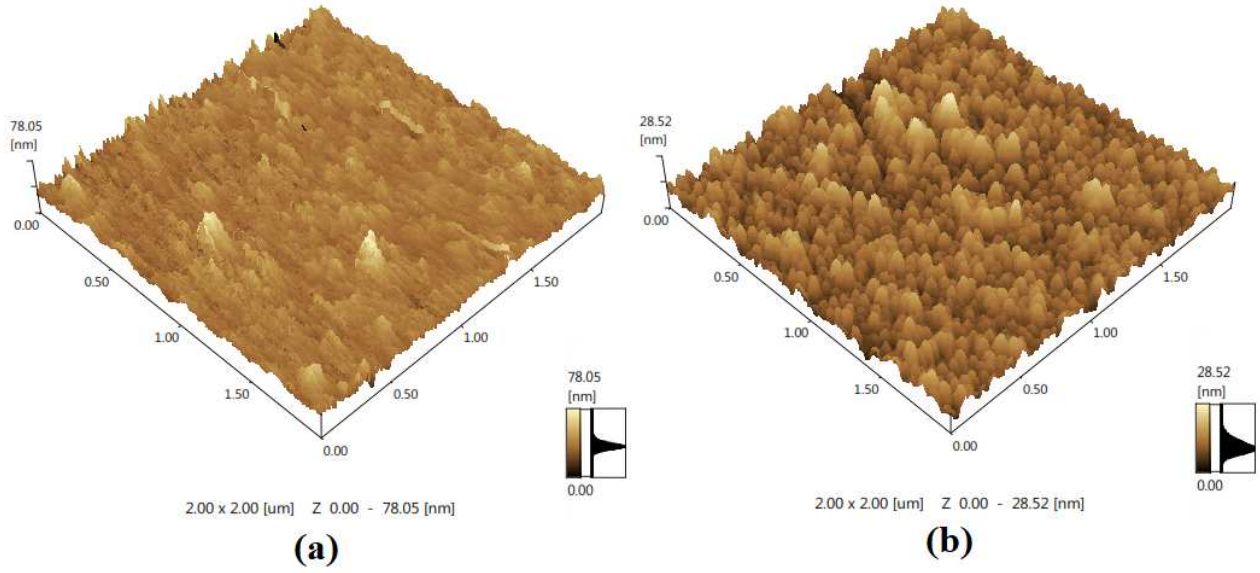


**Figure 4. Three dimensional AFM images of ZnO:Al thin films: a) AZO-1 and b) AZO-2**

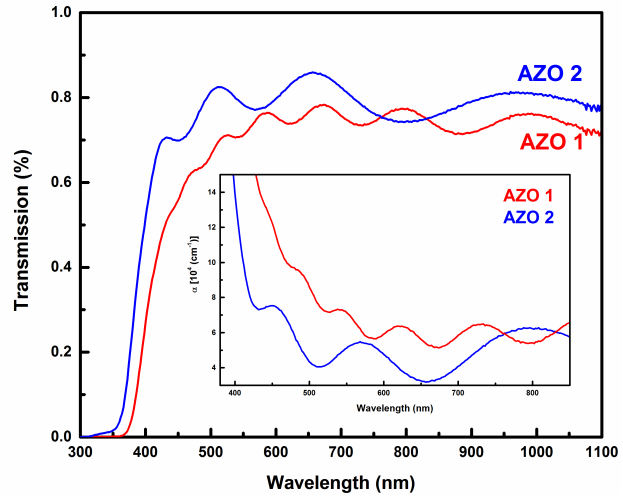


**Figure 5. Optical transmittance spectra for deposited AZO thin films**

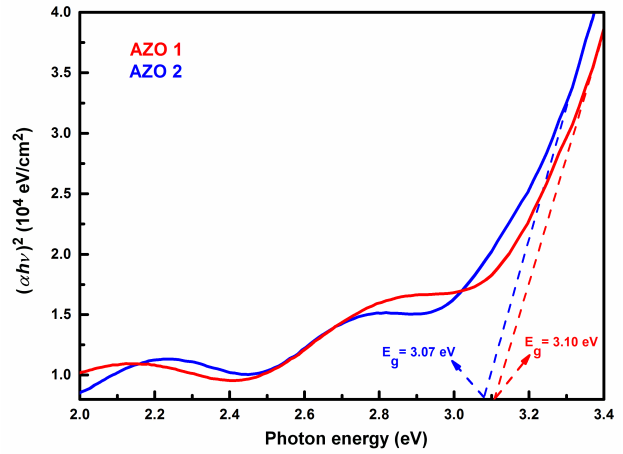


**Figure 6. Tauc plots for deposited ZnO:Al thin films**

the direct transition of the AZO is determined by the Tauc equation [40]:

$$\alpha \cdot h \cdot \nu = A\left(h \cdot \nu - E_g\right)^n \tag{3}$$

where $h \cdot \nu$ is the photon energy, $\alpha$ is the absorption coefficient and $A$ is the constant. The energy of the band gap can be obtained by extrapolating the linear part of the curve to $\alpha \cdot h \cdot \nu = 0$. The exponent $n$ characterizes the type of transition between the energy bands and it can assume the values: 2, 3, ½, and ⅔ for prohibited electronic transitions either direct or indirect type.

Figure 6 presents the Tauc graphic, $(\alpha \cdot h \cdot \nu)^2$ in function of $h \cdot \nu$, with the band gap energy values of the AZO thin films deposited with different electric currents. The ZnO doped with Al was considered a direct band gap material and the experimental values of optical absorption were measured considering $n = 2$. Thus, it is possible to conclude that the electronic transitions are direct.

The value of the optical band gap energy interval suffered a slight decrease with the increase of the deposition electric current, from 0.3 to 0.4 A. The increase in thin film thickness leaves the margin of the spectrum of optical transmittance more accentuated, indicating the formation of a structure with the low concentration of structural defects [41].

### *3.3. Theoretical result*

#### *Crystal structure*

From the experimentally determined lattice parameters for the ZnO unit cell with hexagonal *P*63*mc* spatial group (wurtzite), calculations for geometrical optimization were carried out and resulted in the unit cell shown in Fig. 7. In order to perform the calculations, experimental values of the AZO-2 structure were taken as reference since it presented better results in the analyses compared to the AZO-1.

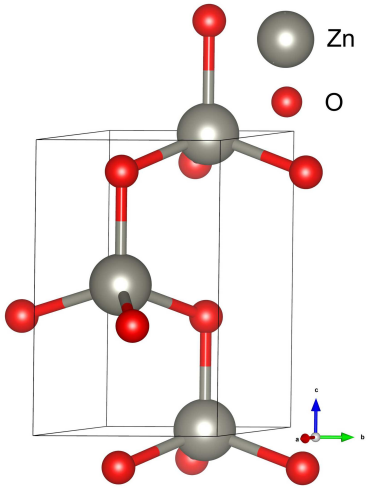


**Figure 7. ZnO unit cell with optimized structure**

Figure 8a presents the 2 × 2 × 2 super cell with spatial group triclinic *P*1, generated from the unit cell of the ZnO with optimized structure, while Fig. 8b shows the 2 × 2 × 2 ZnO super cell doped with 2% of the Al (ZnO:Al) that corresponds to the stoichiometric values of $Zn_{(0.9375)}$, $Al_{(0.0625)}$ and O.

In order to investigate the doping effect on the crystalline structure, the total energies ($E$), formation energy ($E_f$) of impurities and lattice parameters for the pure ZnO and ZnO:Al with optimized geometry, were calculated and the results are given in Table 2. According to the results, the optimized lattice parameters of the pure ZnO are in accordance with the experimental values from the literature [22–24].

The calculations reveal that the lattice parameters and equivalent volumes of the crystal cell decrease slightly after doping. The ionic radius of $Al^{3+}$ (0.53 Å) is smaller than the ionic radius of $Zn^{2+}$ (0.74 Å), thus when $Zn^{2+}$ is replaced by $Al^{3+}$ it leads to a decrease in the Al–O bond length that causes a decrease in the lattice and volume parameters. The difficulty in the doping process of ZnO (wurtzite), in relation to different ions, can be analysed by comparing the formation energies of impurities added in the structure. The doping process would be effi-

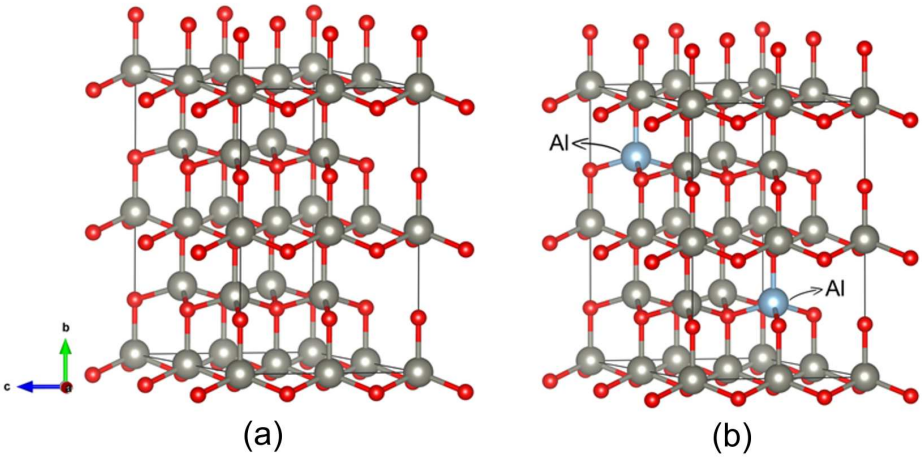


**Figure 8. 2×2×2 supercell of ZnO (a) and doped ZnO:Al (b)**

**Table 2. Total ($E$) and formation ($E_f$) energy values and lattice parameters of the pure ZnO and ZnO:Al**

| | Experimental ZnO:Al | Theoretical ZnO | Theoretical ZnO:Al |
|---|---|---|---|
| $E$ [eV] | | −4294.64 | −4090.48 |
| $E_f$ [eV] | | 3.341 | 3.223 |
| $a = b$ [Å] | 3.2493 | 3.2832 | 3.2545 |
| $c$ [Å] | 5.2054 | 5.2989 | 5.2056 |
| $c/a$ | 1.6020 | 1.6139 | 1.5995 |
| $\alpha = \beta$ [°] | 90 | 90 | 90 |
| $\gamma$ [°] | 120 | 120 | 120 |
| $V$ [Å$^3$] | 47.5948 | 49.4675 | 49.2864 |

**Table 3. Mulliken bond populations and bond lengths of the pure ZnO and ZnO:Al**

| | Bond | Population | Bond length [nm] |
|---|---|---|---|
| ZnO | Zn–O (∥ $c$) | 0.45 | 0.1992 |
| | Al–O (⊥ $c$) | 0.45 | 0.1974 |
| ZnO:Al | Zn–O around Al (∥ $c$) | 0.32 | 0.2004 |
| | Zn–O (⊥ $c$) | 0.28 | 0.2059 |
| | Al–O (∥ $c$) | 0.50 | 1.7914 |
| | Al–O (⊥ $c$) | 0.50 | 1.8132 |

cient and result in a stable structure if the formation and total energies are not very different from the pure ZnO energies, otherwise the structure may not form due to instability. According to the results, the formation energy of the ZnO:Al decreases in relation to the pure ZnO, suggesting a certain easiness in the Al-doping process. However, this causes a substantial increase in the total energy of the ZnO:Al, indicating that it becomes less stable than the pure ZnO.

*Mulliken bond populations*

The Mulliken bonding population provides an objective criterion for the bonding between atoms. The overlapping population can be used to assess the covalent or ionic nature of a bond. High in the bond population indicates a predominantly covalent bond, while a low value indicates a predominantly ionic interaction. Another measure of ionic character can be obtained from the effective ionic valence, which is defined as the difference between the formal ionic load and Mulliken's load on the anionic species. A zero value indicates a perfectly ionic bond, while values greater than zero indicate increasing covalent levels [23].

The Mulliken bonding population is an important method used to analyse the situation of the bond, load distribution and load transfer. The Mulliken bonding population and bond length of ZnO and ZnO:Al are shown in Table 3. For the ZnO the Mulliken bond population and the Zn–O bond length parallel to the $c$-axis direction are 0.4400 and 0.1991 nm, respectively. For the Zn–O bond perpendicular to the $c$-axis those same parameters are 0.4100 and 0.1974 nm, respectively. This indicates that the covalent character of the Zn–O bonds parallel to the $c$-axis direction is stronger than for the bonds perpendicular to the $c$-axis. In the case of ZnO:Al, according to the results, the population of Zn–O bonds becomes lower, while the bond length increases significantly. This can be associated with the difference in atomic radii between $Zn^{2+}$ and $Al^{3+}$. The atomic radius of the $Zn^{2+}$ is greater than the $Al^{3+}$, resulting in the increase in the number of O atoms most distant from the Zn atom, thus, forming longer Zn–O bonds. At the same time, the population of Zn–O bonds decreases, indicating that their covalent character has become weaker. On the other hand, the Al–O bonding population becomes large, indicating that their covalent character became stronger while the ionic bond became weaker. These results corroborate with the results obtained by X-ray diffraction, which show the growth of the crystals in direction of $c$-axis for the unit cell.

*Energy band structure*

The band structure is the model that makes it possible to explain the primary physical properties and the design of high-performance devices in semiconductors and other materials. Figure 9 shows the results of the calculations for the electronic structure of the pure ZnO and ZnO:Al doped samples. The Fermi energy level

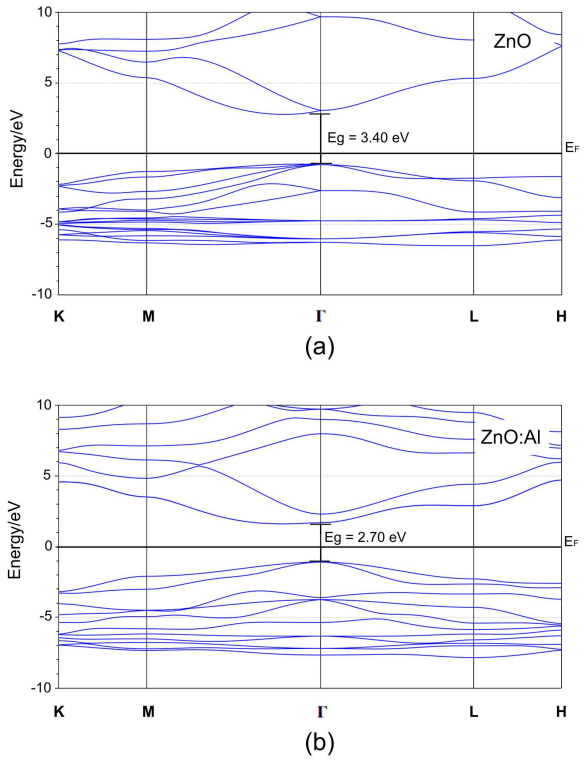


**Figure 9. Band structure of: a) ZnO and b) ZnO:Al**

(EF) is the reference for zero energy, represented by the dashed black line. The band structures of the pure ZnO and ZnO:Al are presented in Figs. 9a and 9b, respectively, in which $E_g$ indicates the band gap, dividing the energies between the valence bands (VB) and conduction bands (CB), respectively. As it can be seen in Fig. 9a, for the pure ZnO, a direct band gap in gamma (Γ) equal to 3.40 eV was obtained, a value close to the experimental result, 3.37 eV [42]. Also, Fig. 9b shows that the ZnO:Al has obtained a direct band gap in Γ equal to 2.70 eV, a value close to the experimental result, 3.07 eV.

These results show that the distance between the valence band and the conduction band has been decreased rapidly as the ZnO is doped, so it is entirely possible to use ZnO:Al for application in solar panels. Furthermore, it confirms that the doping process is efficient, since the values of the formation energies are not very different from the energy values of the pure ZnO, allowing to obtain a stable structure. These results imply that the methods applied are reliable and the calculations are in accordance with the experimental results.

## IV. Conclusions

The transparent conductive thin films were deposited with success by the magnetron sputtering technique on glass substrates. The technique allowed the incorporation of aluminium in the ZnO lattice in an assertive way. The control over the surface morphology, crystallinity and optical transmission of the films was dependent on the values of the deposition current. The computational analyses were performed in order to highlight the effect of structural and electronic changes induced by the Al doping in ZnO and they showed that the lattice parameters and super cell are close to the experimental values of this and other studies. Also, it was possible to observe that with the substitution of $Zn^{2+}$ by $Al^{3+}$, there is a decrease in the Al–O bond length causing the decrease in the lattice and volume parameters. This causes a decrease in the formation energy after doping, indicating that ZnO:Al doping becomes easier. However, it increases the equivalent total energy, pointing out that the doping model becomes less stable than the pure ZnO. In addition, doping allows the electrons of the ZnO:Al to have better transport behaviour and lower ionization energy, due to the decrease of the ionic character of the bonds and an increase in their covalent character. All of these results are reflected in the calculations of the band structure, since the band gap of the pure ZnO of 3.40 eV shifted to 2.70 eV in the ZnO:Al with only 2% of Al substitution. These properties make AZO films deposited by magnetron sputtering suitable for many optoelectronic applications, such as transparent conductive oxides for electronic devices and solar cells. Therefore, the results reported in this work highlight a new approach for future studies that aim to optimize low temperature deposition processes compatible with heat sensitive substrates, preferentially for flexible solar cell platforms or other electronic applications.

**Acknowledgement:** This study was financed in part by the Coordenação de Aperfeiçoamento de Pessoal de Nível Superior - Brasil (CAPES) - Finance Code 001.

## References

1. Y. Zhang, Z. Wu, P. Li, L.K. Ono, Y. Qi, J. Zhou, H. Shen, C. Surya, Z. Zheng, "Fully solution-processed TCO-free semitransparent perovskite solar cells for tandem and flexible applications", *Adv. Energy Mater.*, **8** [1] (2018) 1701569.
2. S. Boscarino, I. Crupi, S. Mirabella, F. Simone, A. Terrasi, "TCO/Ag/TCO transparent electrodes for solar cells application", *Appl. Phys. A*, **116** [3] (2014) 1287–1291.
3. M. Grundmann, "Transparent conductive oxide semiconductors", p. 579 in *The Physics of Semiconductors*, Springer, Cham, 2016.
4. E.L. Pankratov, E.A. Bulaeva, "Doping of materials during manufacture p–n-junctions and bipolar transistors. Analytical approaches to model technological approaches and ways of optimization of distributions of dopants", *Rev. Theor. Sci.*, **1** [1] (2013) 58–82.
5. L. Zhang Y. Zhou, L. Guo, W. Zhao, A. Barnes, H.T. Zhang, C. Eaton, Y. Zheng, M. Brahlek, H.F. Haneef, N.J. Podraza, M.H.W. Chan, V. Gopalan, K.M. Rabe, R. Engel-Herbert, "Correlated metals as transparent conductors", *Nature Mater.*, **15** [2] (2016) 204–210.
6. A. Rayerfrancis, P.B. Bhargav, N. Ahmed, S. Bhattacharya, B. Chandra, S. Dhara, "Sputtered AZO thin films for TCO and back reflector applications in improving the efficiency of thin film a-Si:H solar cells", *Silicon*, **9** [1] (2017) 31–38.

7. K.-M. Lin, R.-L. Lin, W.-T. Hsiao, S.-W. Wu, C.-Y. Chou, Y.-C. Kang, "Development of hybrid transparent electrodes for flexible optoelectronic applications", *8th International Conference on Advanced Materials Development & Performance*, Pune, India 2017.
8. M. Nasiri, S.M. Rozati, "Muscovite mica as a flexible substrate for transparent conductive AZO thin films deposited by spray pyrolysis", *Mater. Sci. Semicond. Process.*, **81** (2018) 38–43.
9. L. Duan, X. Zhao, Y. Zhang, J. Zhou, T. Zhao, W. Geng, "Transparent and conducting Ga doped ZnO films on flexible substrates prepared by sol gel method", *J. Mater. Sci. Mater. Electron.*, **28** [12] (2017) 8669–8674.
10. O.K. Echendu, F.B. Dejene, I.M. Dharmadasa, "An investigation of the influence of different transparent conducting oxide substrates/front contacts on the performance of CdS/CdTe thin-film solar cells", *J. Mater. Sci. Mater. Electron.*, **28** (2017) 18865–18872.
11. Z.B. Ayadi, H. Mahdhi, K. Djessas, J.L. Gauffier, L.E. Mir, S. Alaya, "Sputtered Al-doped ZnO transparent conducting thin films suitable for silicon solar cells", *Thin Solid Films*, **553** (2014) 123–126.
12. Z. Ghorannevis, E. Akbarnejad, A. Salar Elahi, M. Ghoranneviss, "Application of RF magnetron sputtering for growth of AZO on glass substrate", *J. Crystal Growth*, **447** [Supplement C] (2016) 62–66.
13. H. Morkoç, Ü. Özgür, *Zinc Oxide: Fundamentals, Materials and Device Technology*. Wiley-VCH, USA, 2009.
14. A. Aprilia, H. Fernando, A. Bahtiar, L. Safriani, R. Hidayat, "Influences of Al dopant atoms to the structure and morphology of Al doped ZnO nanorod thin film", *J. Phys. Conf. Ser.*, **1080** [1] (2018) 012009.
15. A. Mallick, D. Basak, "Revisiting the electrical and optical transmission properties of co-doped ZnO thin films as n-type TCOs", *Prog. Mater. Sci.*, **96** (2018) 86–110.
16. A. Mallick, D. Basak, "Comparative investigation on cation-cation (Al-Sn) and cation-anion (Al-F) co-doping in RF sputtered ZnO thin films: Mechanistic insight", *Appl. Surface Sci.*, **410** (2017) 540–546.
17. S. Karthick, J.J. Ríos-Ramírez, S. Chakaravarthy, V.S., "Electrical, optical, and topographical properties of RF magnetron sputtered aluminum-doped zinc oxide (AZO) thin films complemented by first-principles calculations", *J. Mater. Sci. Mater. Electron.*, **29** [18] (2018) 15383–15395.
18. H. Mahdhi, Z.B. Ayadi, S. Alaya, J.L. Gauffier, K. Djessas, "The effects of dopant concentration and deposition temperature on the structural, optical and electrical properties of Ga-doped ZnO thin films", *Superlattice. Microst.*, **72** (2014) 60–71.
19. O.K. Alexeeva, V.N. Fateev, "Application of the magnetron sputtering for nanostructured electrocatalysts synthesis", *Int. J. Hydrogen Energy*, **41** [5] (2016) 3373–3386.
20. I.O. Nascimento, "Construction of an experimental apparatus for in situ monitoring of thin film deposition by magnetron sputtering titanium", *M.Sc. thesis*, Universidade Federal do Rio Grande do Norte, Natal, Brazil, 2011.
21. S. Shi, G. He, M. Zhang, X. Song, J. Li, X. Wang, J. Cui, X. Chen, Z. Sun, "Microstructural, optical and electrical properties of molybdenum doped ZnO films deposited by magnetron sputtering", *Sci. Adv. Mater.*, **4** [2] (2012) 193–198.
22. H. Benzarouk, A. Drici, M. Mekhnache, A. Amara, M. Guerioune, J. Christian, "Effect of different dopant elements (Al, Mg and Ni) on microstructural, optical and electrochemical properties of ZnO thin films deposited by spray pyrolysis (SP)", *Superlattice. Microst.*, **52** [3] (2012) 594–604.
23. M.D. Segall, R. Shah, C.J. Pickard, M.C. Payne, "Population analysis of plane-wave electronic structure calculations of bulk materials", *Phys. Rev. B*, **54** [23] (1996) 16317–16320.
24. B. Benhaoua, A. Rahal, S. Benramache, "The structural, optical and electrical properties of nanocrystalline ZnO:Al thin films", *Superlattice Microst.*, **68** (2014) 38–47.
25. J.P. Perdew, K. Burke, M. Ernzerhof, "Generalized gradient approximation made simple", *Phys. Rev. Lett.*, **77** [18] (1996) 3865–3868.
26. H.J. Monkhorst, J.D. Pack, "Special points for Brillouin-zone integrations", *Phys. Rev. B*, **13** [12] (1976) 5188–5192.
27. N. Troullier, J.L. Martins, "Efficient pseudopotentials for plane-wave calculations", *Phys. Rev. B*, **43** [3] (1991) 1993–2006.
28. K. Momma, F. Izumi, "VESTA 3 for three-dimensional visualization of crystal, volumetric and morphology data", *J. Appl. Crystallogr.*, **44** [6] (2011) 1272–1276.
29. C.H. Tseng, W.H. Wang, H.C. Chang, C.P. Chou, C.Y. Hsu, "Effects of sputtering pressure and Al buffer layer thickness on properties of AZO films grown by RF magnetron sputtering", *Vacuum*, **85** [2] (2010) 263–267.
30. B. Sarma, D. Barman, B.K. Sarma, "AZO (Al:ZnO) thin films with high figure of merit as stable indium free transparent conducting oxide", *App. Surface Sci.*, **479** (2019) 786–795.
31. N. Matsunami, O. Fukuoka, M. Tazawa, M. Sataka, "Electronic structure modification of ZnO and Al-doped ZnO films by ions", *Surface Coatings Technol.*, **196** [1] (2005) 50–55.
32. T.-H. Chen, T.-C. Cheng, Z.-R. Hu, "The electrical and optical properties of AZO thin film under different post-annealing temperatures", *Microsyst. Technol.*, **19** [11] (2013) 1787–1790.
33. Y. Chen, S.Y. Ma, "Preparation and photoluminescence studies of high-quality AZO thin films grown on ZnO buffered Si substrate", *Mater. Lett.*, **162** (2016) 75–78.
34. D.-Y. Chen, J.-Y. Kao, C.-Y. Hsu, C.-H. Tsai, "The effect of AZO and compact $TiO_2$ films on the performance of dye-sensitized solar cells", *J. Electroanal. Chem.*, **766** (2016) 1–7.
35. T.K. Subramanyam, P. Goutham, S. Pavan Kumar, S.R. Yadhuraj, K.S. Geetha, "Optimization of sputtered AZO thin films for device application", *Mater. Today Proceed.*, **5** [4, Part 3] (2018) 10851–10859.
36. C.-A. Tseng, J.-C. Lin, Y.-F. Chang, S.-D. Chyou, K.-C. Peng, "Microstructure and characterization of Al-doped ZnO films prepared by RF power sputtering on Al and ZnO targets", *Appl. Surface Sci.*, **258** [16] (2012) 5996–6002.
37. A. Spadoni, M.L. Addonizio, "Effect of the RF sputtering power on microstructural, optical and electrical properties of Al doped ZnO thin films", *Thin Solid Films*, **589** (2015) 514–520.
38. V. Senthilkumar, P. Vickraman, M. Jayachandran, C. Sanjeeviraja, "Structural and optical properties of indium tin oxide (ITO) thin films with different compositions prepared by electron beam evaporation", *Vacuum*, **84** [6]

(2010) 864–869.
39. C. Zegadi, A. Abderrahmane, D. Chaumont, Y. Lacroute, K. Abdelkebir, S. Hamzaoui, M. Adnane, "Influence of iron doping on morphological, structural and optical properties of zinc oxide thin films prepared by dip-coating method", *Surf. Eng. Appl. Electrochem.*, **52** [4] (2016) 362–369.
40. H. Tong, Z. Deng Z. Liu, C. Huang, J. Huang, H. Lan, C. Wang, Y. Cao, "Effects of post-annealing on structural, optical and electrical properties of Al-doped ZnO thin films", *Appl. Surface Sci.*, **257** [11] (2011) 4906–4911.
41. P. Prepelita, V. Craciun, F. Garoi, A. Staicu, "Effect of annealing treatment on the structural and optical properties of AZO samples", *Appl. Surface Sci.*, **352** (2015) 23–27.
42. S. Jiang, J. Xu, D. Miao, L. Peng, S. Shang, P. Zhu, "Water-repellency, ultraviolet protection and infrared emissivity properties of AZO film on polyester fabric", *Ceram. Int.*, **43** [2] (2017) 2424–2430.